PCCP

PAPER

View Article Online
View Journal | View Issue



Cite this: *Phys. Chem. Chem. Phys.*, 2015, **17**, 27409

# Interaction at the silicon/transition metal oxide heterojunction interface and its effect on the photovoltaic performance†

Zhimin Liang,[a] Mingze Su,[a] Yangyang Zhou,[a] Li Gong,[b] Chuanxi Zhao,[a] Keqiu Chen,[a] Fangyan Xie,[b] Weihong Zhang,[b] Jian Chen,[b] Pengyi Liu[a] and Weiguang Xie*[a]

Received 6th September 2015,
Accepted 20th September 2015

DOI: 10.1039/c5cp05309a

www.rsc.org/pccp

The interfacial reaction and energy level alignment at the Si/transition metal oxide (TMO, including $MoO_{3-x}$, $V_2O_{5-x}$, $WO_{3-x}$) heterojunction are systematically investigated. We confirm that the interfacial reaction appears during the thermal deposition of TMO, with the reaction extent increasing from $MoO_{3-x}$, to $V_2O_{5-x}$, and to $WO_{3-x}$. The reaction causes the surface oxidation of silicon for faster electron/hole recombination, and the reduction of TMO for effective hole collection. The photovoltaic performance of the Si/TMO heterojunction devices is affected by the interface reaction. $MoO_{3-x}$ are the best hole selecting materials that induce least surface oxidation but strongest reduction. Compared with H-passivation, methyl group passivation is an effective way to reduce the interface reaction and improve the interfacial energy level alignment for better electron and hole collection.

Although silicon solar cells are the most mature devices in the photovoltaic market, they still suffer from their low light absorption coefficient and high fabrication cost. Intense studies have focused on improving the light trapping using the textured surface.[1–3] Besides, as the hole mobility is smaller than the electron mobility in silicon, replacing p-type Si using a novel hole selective layer is another important topic. Hybrid silicon nanowire (SiNW) photovoltaic devices using a low cost, solution process organic layer, for example PEDOT:PSS, have shown an efficiency of 13.7%.[4,5] By using conductive carbon nanotubes as the hole transporting layer, Jung *et al.* also showed a silicon heterojunction solar cell with efficiency better than 10%.[6] In the studies of organic solar cells, transition metal oxides (TMOs), for example, $MoO_{3-x}$, have been extensively used as hole selective layers to enhance the device performance.[7] In recent years, the application of TMOs in Si solar cells has also been demonstrated.[8–11] Battaglia *et al.* show that by hydrogenating the surface of n-Si and carefully controlling the stoichiometry of $MoO_{3-x}$, the performance of n-Si/$MoO_{3-x}$ can be greatly improved.[12] $MoO_x$-based heterojunction silicon solar cells with power conversion efficiency (PCE) as high as 22.5% were just demonstrated by Geissbühler *et al.*[13] It shows the promising future of using low-cost TMOs as conducting layers in commercialized solar cells.

Although high PCE has been demonstrated, forming a Si/TMO contact is complex. First, the properties of the silicon surface are sensitive to the oxygen amount. Yang *et al.* have shown that when an intrinsic a-Si:H layer was deposited on the $MoO_3$ surface, inter-diffusion of oxygen into the a-Si:H takes place. The PCE of the devices decreases rapidly in the first 10 hours.[10] Thermally deposited $MoO_x$ on the a-Si:H layer is expected to minimize the oxidation effect, however, Battaglia *et al.* observed a slight S shape *J–V* curve in their high efficient $MoO_x$/a-Si:H/c-Si heterojunction.[14] They suggested that it came from the misalignment of the interfacial energy levels. The results imply that hydrogen passivation may not be an efficient passivation method for the silicon/TMO heterojunction. In recent studies, other passivation methods, for example, methyl groups ($-CH_3$), have been shown to improve the mobility and stability of SiNWs.[15] Zhang *et al.* showed an air stable $CH_3$-passivated Si/P3HT hybrid solar cell with a PCE of 5.9%.[16] Liang *et al.* further confirmed the stability of the interfacial energy band using cross-sectional Kelvin probe force microscopy (KPFM).[17] Whether the other passivation method is applicable for the Si/TMO heterojunction is unknown. Second, the properties of TMOs are also sensitive to the oxygen deficiency. Photoelectron emission spectroscopy experiments have shown that the band structure of TMOs has strong correlation with the oxidation states of the metal atoms.[18] Moreover, the oxidation state depends strongly on the substrate in the first

[a] *Siyuan Laboratory, Department of Physics, Jinan University, Guangzhou, Guangdong, 510632, P. R. China. E-mail: wgxie@email.jnu.edu.cn*
[b] *Instrumental Analysis & Research Center, Sun Yat-sen University, Guangzhou, 510275, P. R. China*

† Electronic supplementary information (ESI) available. See DOI: 10.1039/c5cp05309a

10 nm, which is just the thickness of TMOs normally used in the Si/TMO heterojunction. Therefore, it is highly required to illustrate the interfacial energy level alignment of the Si/TMO heterojunction and its dependence on the junction formation process.

In this study, thermal deposition of TMOs, including $MoO_3$, $WO_3$ and $V_2O_5$, on the silicon surface was investigated. The interfacial reaction at the Si/TMO heterojunction was confirmed and its effect on the electronic structure of both silicon and TMOs sides was revealed using XPS/UPS. The surface passivation effect by $-CH_3$ groups and hydrogen was compared. Details of the interfacial energy level alignment of the Si/TMO heterojunction were quantitatively studied and its relationship with the photovoltaic performances is discussed.

The n-type (100) double polished crystal Si wafers with a resistivity of 0.5–0.9 Ω cm were ultrasonically cleaned in acetone, ethanol and deionized water in sequences for 15 min separately. The substrate was then cleaned in a piranha solution at 80 °C for 30 min and rinsed with deionized water. A pyramidal structure was obtained on the clean Si wafer by anisotropic etching using 0.2 wt% sodium hydroxide and 10 wt% ethanol at 80 °C for 30 min. Then the substrate was immersed in the diluted hydrochloric acid to remove the residual alkali and cleaned with deionized water.[19] The surface hydrogen passivation was obtained by soaking the substrate in a HF solution (5 M) for 10 min. To prepare the $CH_3$-terminated surface, the surface is first passivated by hydrogen and then transferred into a glove box immediately. The substrate was then immersed in a chlorobenzene (CB) solution of superfluous phosphorus pentachloride ($PCl_5$) at 100 °C for 1 h. Then the sample was cleaned with CB and tetrahydrofuran (THF) and immersed in a solution of $CH_3MgCl$ (1 M) in THF at 80 °C for 8 h. The $CH_3$-terminated surface was formed after the sample was rinsed with THF and methyl alcohol.[17] A 200 nm-thick aluminum electrode was deposited on the back side of the Si substrate as a rear electrode by thermal evaporation. Three types of TMO ($MoO_{3-x}$, $V_2O_{5-x}$, $WO_{3-x}$) thin films with a thickness of 10 nm were deposited on the surface of Si substrate by thermal evaporation at a pressure of $5 \times 10^{-6}$ mbar. Silver grids with a thickness of 100 nm were deposited on the surface of TMO thin films by thermal evaporation as the top electrode through a shadow mask. The effective device area is $2.5 \times 4$ mm$^2$. The surface band structure was measured by X-ray photoelectron emission spectroscopy (XPS) and ultra-violet photoelectron emission spectroscopy (UPS) using a Thermo VG ESCALAB 250 photoelectron spectrometer. All the photovoltaic *J–V* characteristics were tested using a Keithley 2400 source meter at 100 mW cm$^{-2}$ irradiation intensity under the condition of AM 1.5G using a sun solar simulator (Abet Technologies).

To investigate the oxidation effect by TMO deposition, we focus on the formation of $SiO_x$ at binding energy between 101 eV and 105 eV. On the as prepared H–Si surface, only the Si 2p3, 2p1 peak corresponding to the crystal Si is observed. On the $CH_3$-passivated surface, there is a small peak at 103.2 eV, which comes from the formation of $SiO_2$. Fig. 1(a) and (c) shows the Si peaks after oxide deposition. As the XPS is only sensitive to surface elements, intensity of peaks from the silicon substrates should decrease dramatically after oxide deposition. However, on the H-passivated surface, new $SiO_x$ peaks were observed between 101 eV and 105 eV. The peaks are also observed on the

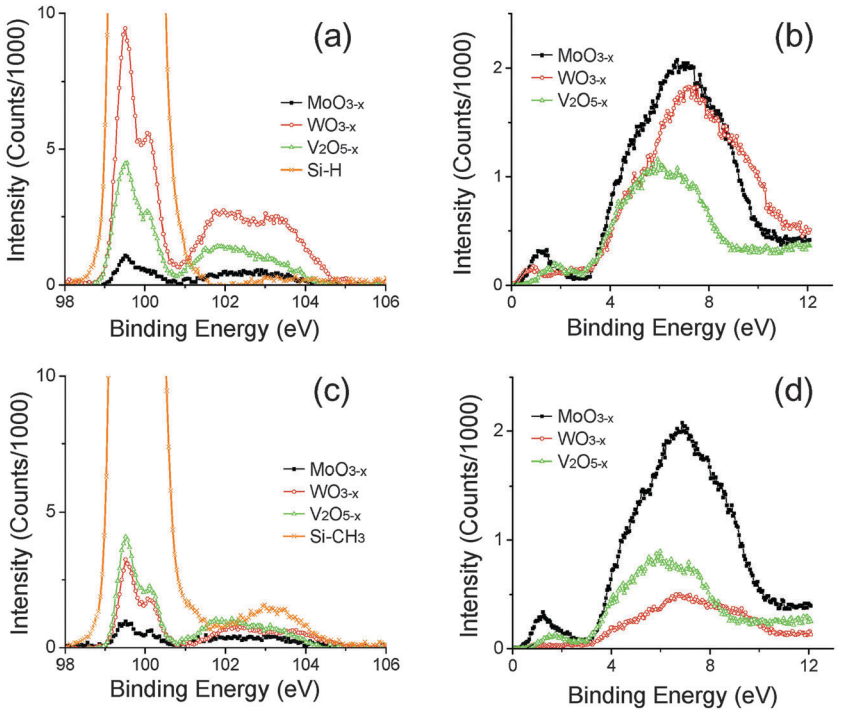


Fig. 1 (a) and (c) The Si 2p peak after deposition of TMOs on the Si–H and Si–$CH_3$ surface respectively; the Si 2p peaks of the as-prepared Si–H and Si–$CH_3$ surface were zoomed in for comparison. (b) and (d) The valance band structure of TMOs on the Si–H and Si–$CH_3$ surface respectively.

 

$CH_3$-passivated surface with intensity close to that observed on the pristine $CH_3$–Si surface. This indicates that during the deposition of TMOs, the silicon will react with the TMOs on the surface, which forms oxidized interfacial layers. It is found that the oxidation effect depends on the types of TMOs. The oxide peak is the smallest on the Si–H/$MoO_{3-x}$ surface. The peak on the Si–H/$V_2O_{5-x}$ is bigger. The oxide peaks are the strongest on the Si–H/$WO_{3-x}$ and a new peak at 101.6 eV corresponding to the formation of SiO can be found. As the deposition temperature was $T_{WO_{3-x}} > T_{V_2O_{5-x}} > T_{MoO_{3-x}}$, we suggest that the formation of $SiO_x$ is caused by the bombardment of hot TMO molecules. Fig. 1(c) shows that on the $CH_3$-passivated surface, the intensity of the oxide peak decreases, especially on Si–$CH_3$/$WO_{3-x}$. It shows that $CH_3$-passivation is efficient to reduce the interfacial oxidation. The passivation effect may be originated from the high temperature stability of Si–$CH_3$ bonding.[20] In addition, the $CH_3$ group is much larger than the H atom. When a TMO molecule is deposited on the $CH_3$ passivated surface, the O atom is more likely to replace the H atom on the $CH_3$ group rather than replacing the $CH_3$ group. The above results show that interfacial oxidation is universe during the deposition of TMOs.

As silicon surface is oxidized during the deposition, it can be expected that the TMO layer is reduced. A small gap state centered at around 1–2 eV was observed (Fig. 1(b) and (d)). The gap states came from the oxygen deficiency in the film, and a higher concentration of oxygen deficiency generates more gap states. From Fig. 1(a) and (c), we can find that the oxidation effect on H-passivated and $CH_3$-passivated surface is similar during deposition of $MoO_{3-x}$, so the reduction effect should be similar. Fig. 1(b) and (d) show that the gap states are similar on both surfaces, which is consistent with the above assumption. It shows that the vacancy formation of $MoO_{3-x}$ is dominated by the thermal evaporation procedure. In contrast, as the oxidation effect on the H-passivated surface is stronger than that of the $CH_3$-passivated surface during the deposition of $WO_{3-x}$, the observed reduction effect of $WO_{3-x}$ is stronger and thus the intensity of the gap states is also stronger. The edge of the gap states moved from 0.63 eV on the $CH_3$-passivated surface to 0.14 eV on the H-passivated surface. The reduction effect can be further confirmed by the change of valance states of the metal ions (Fig. S1, ESI†). It is found that the changes in 3d states of $MoO_{3-x}$ on both surfaces are very small. However, 3f states of $WO_{3-x}$ on both surfaces are different. A clear peak at around 35 eV can be observed on the H-passivated surface, which comes from the reduction of $W^{6+}$ to $W^{5+}$. The results confirmed that during thermal deposition of TMOs, interfacial reaction causes the oxidation of silicon and the reduction of TMO, which alters the electronic states of both materials.

Fig. 2(a) shows the electronic states of the H-passivated and $CH_3$-passivated silicon surface respectively. The accurate surface band bending can be calculated by comparing the difference of $E_{Si} - E_{VBM}$ between the surface and the bulk (Table 1). The bulk value of $(E_{Si} - E_{VBM})_{bulk}$ has a specific value of 98.74 eV.[20] The surface $(E_{Si} - E_{VBM})_{CH_3}$ is 98.83 eV, and the $(E_{Si} - E_{VBM})_H$ is 98.60 eV, which give an upward band bending of 0.10 eV for the as-prepared $CH_3$-terminated surface and the downward band bending of −0.14 eV for the as-prepared H-terminated surface.

To figure out the interfacial energy level alignment, the UPS high energy cut-off of the silicon surface after passivation and deposition of TMOs is shown in Fig. 2(b) and (c). The work functions can be determined from the cut-off edge, which are 4.04 eV for the hydrogen passivated surface and 3.84 eV for the $CH_3$-passivated surface. This confirmed that the surface passivation has led to a strong dipole layer on the surface of n-Si.[20] Further deposition of $MoO_{3-x}$ on the silicon surface shows a work function of 4.70 eV for the Si–H/$MoO_{3-x}$ structure and 4.55 eV for the Si–$CH_3$/$MoO_{3-x}$ structure respectively. This observed work function is much smaller than $MoO_{3-x}$ films deposited on other substrates,[12] which means that their electronic states in the device structure are strongly affected by the surface dipole of Si. The same phenomenon is observed for other TMO layers. According to the above measurements, the energy band diagram at the interface can be constructed. Fig. 3(a) and (b) shows the typical example of $MoO_{3-x}$. As the

Table 1 Band bending of the Si surface, the unit is eV

| | Si 2p3 | VBM | Diff. | Diff. − 98.74 (bulk) |
|---|---|---|---|---|
| Si—H | 99.51 | 0.91 | 98.60 | −0.14 |
| Si–$CH_3$ | 99.51 | 0.67 | 98.84 | 0.10 |

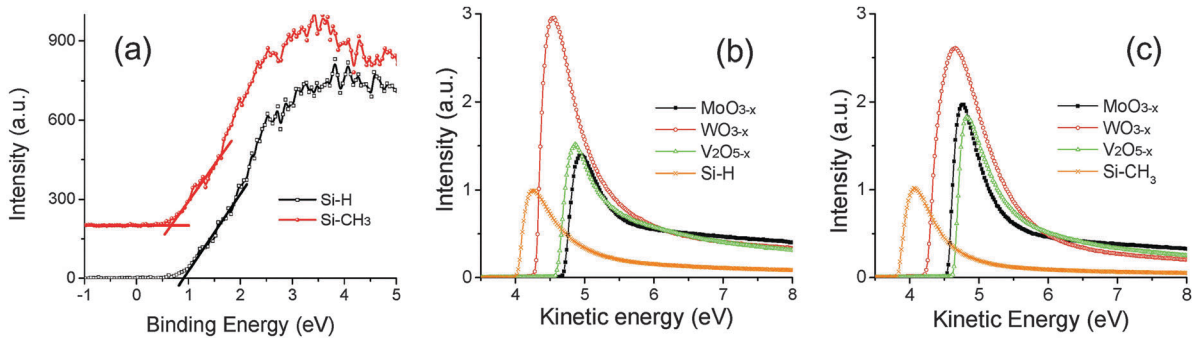


Fig. 2 (a) The valance spectra of the as-prepared Si–H and Si–$CH_3$ surface. (b) and (c) The high energy cut-off of Si and TMO/Si with a H-passivated and a $CH_3$-passivated surface respectively.

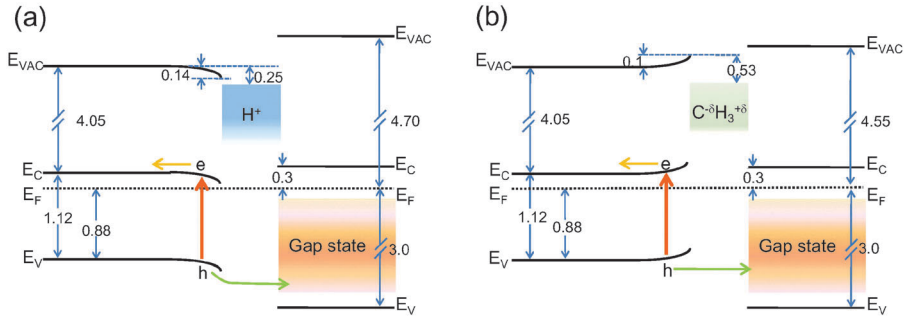


Fig. 3 The energy level alignment at the Si/$MoO_{3-x}$ interface: (a) the H-passivated surface; (b) the $CH_3$-passivated surface.

interface is less affected by the oxidation effect, the value of energy band bending is assumed to be the same in Table 1.

From the energy diagram in Fig. 3, when the heterojunction is illuminated, the electron–hole pairs will be generated and separated in the n-Si side. To effectively collect the carriers, electrons are expected to flow out of the n-Si side and the holes from the $MoO_{3-x}$ side. The valance band of $MoO_{3-x}$ locates at $E_F - 3.0$ eV. It does not match the valance band of silicon. Instead, the gap state with an edge at 0.55 eV seems to be favorable for hole transport, which is consistent with former studies on organic solar cells.[21,22] The collection efficiency depends on three parameters: a high electron barrier from n-Si to $MoO_{3-x}$, a low hole barrier from n-Si to $MoO_{3-x}$ and a high built-in potential for electron and hole extraction. From Fig. 3(a), the constraint in the Si–H/$MoO_{3-x}$ lies at the downward band bending. This will form a reverse electrical field that will raise the barriers for holes to be transferred out from the $MoO_{3-x}$ side. It will also cause the reverse diffusion of electrons to the interface, which will lead to faster recombination at the interface. However, it can be found from Fig. 3(b) that the upward band bending of the $CH_3$-passivated surface is more favorable for blocking the reverse diffusion of electrons and the extraction of holes.

Heterojunction photovoltaic devices with a structure of Al/Si/10 nm TMO/Ag devices are shown in Fig. 4. We first consider the Si/$MoO_{3-x}$ device. The Si–H/$MoO_{3-x}$ device has a PCE of 6.2%, with an open-circuit voltage ($V_{OC}$) of 0.48 V, a short-circuit current density ($J_{SC}$) of 26.6 mA $cm^{-2}$ and a fill factor (FF) of 48.4%. The Si–$CH_3$/$MoO_{3-x}$ device shows a better PCE of 9.4%, with a $V_{OC}$ of 0.50 V, a $J_{SC}$ of 36.1 mA $cm^{-2}$ and a FF of 51.7%. A significant improvement of the device performance is consistent with the improvement of the interfacial energy level alignment as discussed above.

Although the energy levels of $WO_{3-x}$ and $V_2O_{5-x}$ are close to that of $MoO_{3-x}$ (Fig. S2, ESI†), the interfacial reaction is stronger, thus their device performances are also affected. On one hand, the oxidation of the silicon surface causes traps that accelerate electron/hole recombination, on the other hand, the reduction of metal oxide induces a gap state for effective hole transportation. Therefore, there is a competition in-between. For the three types of devices, Si–H/$MoO_{3-x}$, Si–H/$V_2O_{5-x}$, and Si–H/$WO_{3-x}$, the interfacial reaction extent increases successively, while the observed photovoltaic performances decrease successively in Fig. 4(b), which suggest that the oxidation effect may be the limiting factor. $CH_3$-pasivation can suppress the interfacial reaction, and thus the effect of oxidation. By replacing the H-passivated surface by the $CH_3$-passivated surface, we observed improved PCE from 5.8% to 7.5% and 5.2% to 7.2% in Si/$V_2O_{5-x}$, and Si/$WO_{3-x}$ devices respectively. However, as the reduction of metal oxide is also suppressed in Fig. 1(d), hole transportation is affected. Therefore, the improvement of the related device performances is also smaller than that of Si/$MoO_{3-x}$ (Fig. 4(c)).

In brief, interface reaction is a universal phenomenon during the deposition of metal oxide on silicon. The oxidation of the silicon surface should be controlled in a small extent for better electron and hole collection. On the contrary, the reduction of TMO is expected for better electron and hole collection. Therefore, there is a consideration of balance between these two effects. $MoO_{3-x}$ is the most widely used TMO materials for the Si/TMO heterojunction and in organic electronics. From our study, we can see that $MoO_{3-x}$ is a good choice because it causes less oxidation

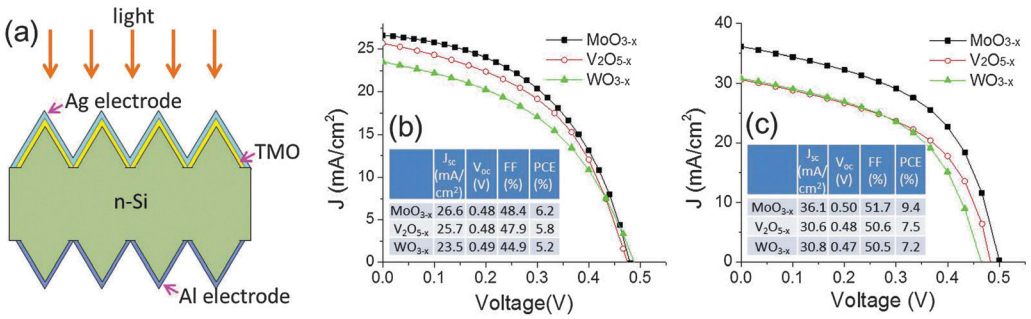


| | $J_{sc}$ (mA/cm²) | $V_{oc}$ (V) | FF (%) | PCE (%) |
|---|---|---|---|---|
| $MoO_{3-x}$ | 26.6 | 0.48 | 48.4 | 6.2 |
| $V_2O_{5-x}$ | 25.7 | 0.48 | 47.9 | 5.8 |
| $WO_{3-x}$ | 23.5 | 0.49 | 44.9 | 5.2 |

| | $J_{sc}$ (mA/cm²) | $V_{oc}$ (V) | FF (%) | PCE (%) |
|---|---|---|---|---|
| $MoO_{3-x}$ | 36.1 | 0.50 | 51.7 | 9.4 |
| $V_2O_{5-x}$ | 30.6 | 0.48 | 50.6 | 7.5 |
| $WO_{3-x}$ | 30.8 | 0.47 | 50.5 | 7.2 |

Fig. 4 (a) Schematic structure of the Al/Si/10 nm TMO/Ag photovoltaic device, and typical photovoltaic performance: (b) Si–H/TMO; (c) Si–$CH_3$/TMO.

 

effects and induced relatively strong gap states for hole extraction. Surface passivation by methyl groups is an effective way to reduce the interfacial reaction and provide better energy level alignment to enhance the photovoltaic effect of the Si/TMO heterojunction. For devices based on $WO_{3-x}$ and $V_2O_{5-x}$, surface passivation is not enough to improve device performance. Additional way that only induces the reduction of the material, such as vacuum annealing or hydrogen injection may be required for further optimization. These findings are helpful to understand the interaction mechanism between TMOs and the substrate, and show special application importance in the design of Si heterojunctions for solar cells.

## Acknowledgements

This work was financially supported by the National Natural Science Foundation of China (Grants No. 11574119, 51303217, 51373205), the Guangdong Natural Science Foundation (Grants No. 2014A030313381, 2014A030310302, S2013010012856) and the Fundamental Research Funds for the Central Universities (Grants No. 21615309).

## References

1 E. Garnett and P. Yang, *Nano Lett.*, 2010, **10**(3), 1082–1087.
2 T. Song, S.-T. Lee and B. Sun, *Nano Energy*, 2012, **1**(5), 654–673.
3 W.-R. Wei, M.-L. Tsai, S.-T. Ho, S.-H. Tai, C.-R. Ho, S.-H. Tsai, C.-W. Liu, R.-J. Chung and J.-H. He, *Nano Lett.*, 2013, **13**(8), 3658–3663.
4 P. Yu, C.-Y. Tsai, J.-K. Chang, C.-C. Lai, P.-H. Chen, Y.-C. Lai, P.-T. Tsai, M.-C. Li, H.-T. Pan, Y.-Y. Huang, C.-I. Wu, Y.-L. Chueh, S.-W. Chen, C.-H. Du, S.-F. Horng and H.-F. Meng, *ACS Nano*, 2013, **7**(12), 10780–10787.
5 Y. Zhang, W. Cui, Y. Zhu, F. Zu, L. Liao, S.-T. Lee and B. Sun, *Energy Environ. Sci.*, 2015, **8**(1), 297–302.
6 Y. Jung, X. K. Li, N. K. Rajan, A. D. Tayor and M. A. Reed, *Nano Lett.*, 2013, **13**(1), 95–99.
7 S. Chen, J. R. Manders, S. W. Tsang and F. So, *J. Mater. Chem.*, 2012, **22**(46), 24202–24212.
8 S. Avasthi, W. E. McClain, G. Man, A. Kahn, J. Schwartz and J. C. Sturm, *Appl. Phys. Lett.*, 2013, **102**(20), 203901.
9 J. Bullock, A. Cuevas, T. Allen and C. Battaglia, *Appl. Phys. Lett.*, 2014, **105**(23), 232109.
10 J.-H. Yang, H.-H. Jung, J. Seo, K.-D. Kim, D.-H. Kim, D.-C. Lim, S.-G. Park, J.-W. Kang, M. Song, M.-S. Choi, J.-D. Kwon, K.-S. Nam, Y. Jeong, S.-H. Kwon, Y. C. Park, Y.-C. Kang, K. B. Chung, C. S. Kim, K. S. Lim and S. Y. Ryu, *J. Phys. Chem. C*, 2013, **117**(45), 23459–23468.
11 R. Liu, S.-T. Lee and B. Sun, *Adv. Mater.*, 2014, **26**(34), 6007–6012.
12 C. Battaglia, X. Yin, M. Zheng, I. D. Sharp, T. Chen, S. McDonnell, A. Azcatl, C. Carraro, B. Ma, R. Maboudian, R. M. Wallace and A. Javey, *Nano Lett.*, 2014, **14**(2), 967–971.
13 J. Geissbühler, J. Werner, S. Martin de Nicolas, L. Barraud, A. Hessler-Wyser, M. Despeisse, S. Nicolay, A. Tomasi, B. Niesen, S. De Wolf and C. Ballif, *Appl. Phys. Lett.*, 2015, **107**(8), 081601.
14 C. Battaglia, S. M. de Nicolás, S. De Wolf, X. Yin, M. Zheng, C. Ballif and A. Javey, *Appl. Phys. Lett.*, 2014, **104**(11), 113902.
15 H. Haick, P. T. Hurley, A. I. Hochbaum, P. D. Yang and N. S. Lewis, *J. Am. Chem. Soc.*, 2006, **128**(28), 8990–8991.
16 F. T. Zhang, B. Q. Sun, T. Song, X. L. Zhu and S. Lee, *Chem. Mater.*, 2011, **23**(8), 2084–2090.
17 Z. M. Liang, M. Z. Su, H. Wang, Y. T. Gong, F. Y. Xie, L. Gong, H. Meng, P. Y. Liu, H. J. Chen, W. G. Xie and J. Chen, *ACS Appl. Mater. Interfaces*, 2015, **7**(10), 5830–5836.
18 M. T. Greiner, L. Chai, M. G. Helander, W.-M. Tang and Z.-H. Lu, *Adv. Funct. Mater.*, 2012, **22**(21), 4557–4568.
19 E. Vazsonyi, K. De Clercq, R. Einhaus, E. Van Kerschaver, K. Said, J. Poortmans, J. Szlufcik and J. Nijs, *Sol. Energy Mater. Sol. Cells*, 1999, **57**(2), 179–188.
20 R. Hunger, R. Fritsche, B. Jaeckel, W. Jaegermann, L. J. Webb and N. S. Lewis, *Phys. Rev. B: Condens. Matter Mater. Phys.*, 2005, **72**(4), 045317.
21 M. Vasilopoulou, A. M. Douvas, D. G. Georgiadou, L. C. Palilis, S. Kennou, L. Sygellou, A. Soultati, I. Kostis, G. Papadimitropoulos, D. Davazoglou and P. Argitis, *J. Am. Chem. Soc.*, 2012, **134**(39), 16178–16187.
22 B. Dasgupta, W. P. Goh, Z.-E. Ooi, L. M. Wong, C. Jiang, Y. Ren, E. S. Tok, J. Pan, J. Zhang and S. Y. Chiam, *J. Phys. Chem. C*, 2013, **117**(18), 9206–9211.